Advanced Beam Formulations for Free-Vibration Analysis of Conventional and Joined Wings

Erasmo Carrera[1]; Marco Petrolo[2]; and Alberto Varello[3]

Abstract: This work extends advanced beam models to carry out a more accurate free-vibration analysis of conventional (straight, or with sweep/dihedral angles) and joined wings. The beam models are obtained by assuming higher-order (up to fourth) expansions for the unknown displacement variables over the cross-section. Higher-order terms permit bending/torsion modes to be coupled and capture any other vibration modes that require in-plane and warping deformation of the beam sections to be detected. Classical beam analyses, based on the Euler-Bernoulli and on Timoshenko beam theories, are obtained as particular cases. Numerical solutions are obtained by using the finite element (FE) method, which permits various boundary conditions and different wing/section geometries to be handled with ease. A comparison with other shell/solid FE solutions is given to examine the beam model. The capability of the beam model to detect bending, torsion, mixed and other vibration modes is shown by considering conventional and joined wings with different beam axis geometries as well as with various sections (compact, plate-type, thin-walled airfoil-type). The accuracy and the limitations of classical beam theories have been highlighted for a number of problems. It has been concluded that the proposed beam model could lead to quasi-three-dimensional dynamic responses of classical and nonclassical beam geometries. It provides better results than classical beam approaches, and it is much more computationally efficient than shell/solid modeling approaches. **DOI: 10.1061/(ASCE)AS.1943-5525.0000130.**

CE Database subject headings: Beams; Finite element method; Vibration; Thin-wall structures; Aerospace engineering.

Author keywords: Beams; Finite element method; Higher-order theories; Vibration; Thin-walled structures; Aerospace engineering.

Introduction

The free-vibration analysis of aircraft wings represents one of the most challenging issues of the design process of aircraft. An appropriate evaluation of natural frequencies and modes plays a fundamental role in analyzing gust responses and aeroelastic phenomena. Wings are generally thin-walled, nonuniform, arbitrary-shaped structures. They are usually tapered and have sweep and/or dihedral angles. All of these features introduce complicated effects that require refined structural modelings.

The structural analysis of an aircraft wing can be dealt with by exploiting different models: one-dimensional (1D) (beams), two-dimensional (2D) (plates/shells), and three-dimensional (3D) (solids). One-dimensional theories are attractive because they generally require less computational effort than the analysis of shells or solids. Some well-known classical beam models are the Euler-Bernoulli (Euler 1744) and Timoshenko (Timoshenko 1921, 1922; Timoshenko and Goodier 1970) models; the latter includes transverse shear-deformation and rotary inertia effects. The applicability of classical beam models becomes imprudent as the importance of the nonclassical effects increases. Typical nonclassical effects in a wing structure are those caused by in- and out-of-plane warping, twisting, bending-torsion coupling, and higher-order shear effects, among others.

Many refined higher-order beam theories with enhanced capabilities have been proposed to overcome the limitations of classical models. A discussion of some significant contributions is given hereafter. An excellent review of several beam and plate theories has been presented by Kapania and Raciti (1989) for vibration, wave propagations, buckling, and postbuckling. Thin- and thick-walled beams were considered. The importance of the shear deformation was pointed out. Bishop et al. (1989) have studied coupled bending-torsion modes of uniform beams by combining the Euler-Bernoulli flexural beam theory with the Saint-Venant torsion theory. They underlined the importance of including warping effects for open-section beams. A higher-order beam theory for the analysis of the bending modes was presented by Senjanović and Fan (1989). Comparisons were made with 2D model results. They underlined the convenience of 1D models compared with more cumbersome 2D models for the analysis of complex thin-walled multicell structures, at least for the mid-frequency domain. The effect of shear-deformation on the natural frequencies of composite beam models for rotor blades has been investigated by Chandrashekhara et al. (1990) by means of a first-order, shear-deformation theory. Arbitrary boundary conditions were considered. Song and Librescu (1993) have addressed the dynamic problem of thick- and thin-walled composite beams. They highlighted the role played by various nonclassical effects in predicting the vibrational behavior of beams. The exact vibration frequencies of asymmetrical laminated beams have been computed by

[1]Professor of Aerospace Structures and Aeroelasticity, Dept. of Mechanical and Aerospace Engineering, Politecnico di Torino, Corso Duca degli Abruzzi 24, 10129 Torino, Italy (corresponding author). E-mail: erasmo.carrera@polito.it

[2]Research Assistant, Dept. of Mechanical and Aerospace Engineering, Politecnico de Torino, Corso Duca degli Abruzzi 24, 10129 Torino, Italy; formerly, Institut Jean Le Rond d'Alembert, UMR7190 CNRS, Paris06, Case 162, Tour 55-65, 4, Place Jussieu, 75252, Paris, France. E-mail: marco.petrolo@polito.it

[3]Ph.D. Student, Dept. of Mechanical and Aerospace Engineering, Politecnico de Torino, Corso Duca degli Abruzzi 24, 10129 Torino, Italy; formerly, Institut Jean Le Rond d'Alembert, UMR7190 CNRS, Paris06, Case 162, Tour 55-65, 4, Place Jussieu, 75252 Paris, France. E-mail: alberto.varello@polito.it

Note. This manuscript was submitted on February 19, 2010; approved on May 10, 2011; published online on May 12, 2011. Discussion period open until September 1, 2012; separate discussions must be submitted for individual papers. This paper is part of the ***Journal of Aerospace Engineering***, Vol. 25, No. 2, April 1, 2012. ©ASCE, ISSN 0893-1321/2012/2-282–293/$25.00.

Eisenberger et al. (1995). General layouts and geometries as well as shear-deformation and rotary inertia effects were considered. Marur and Kant (Marur and Kant 1996; Kant et al. 1997) have proposed a model that does not require a shear correction coefficient. Cubic axial and quadratic shear strain variations on the cross-section were used. The free-vibration and transient analyses of laminated beams were conducted. They showed that the higher-order models furnish lower frequencies; that is, a more flexible structure is modeled by the refined theories. The importance of transverse shear and in- and out-of-plane warping in the dynamic analyses of composite beam has been underlined by McCarthy and Chattopadhy (1998). A comparison of classical and refined beam theories for buckling and free-vibration analyses of laminated structures has been made by Song and Waas (1997). It was shown that, whereas the Euler-Bernoulli model represents a first-order solution, the Timoshenko model furnishes solutions that lie outside the bounds of the classical elasticity solution. Dancila and Armonios (1998) have presented a solution procedure to deal with the coupling of extension, bending, and twist vibration modes of slender thin-walled composite beams with particular interest for dynamic and aeroelastic applications. The influence of the beam length on the coupling effects was highlighted. The flexural frequencies of composite beams have been investigated by Shi and Lam (1999). They used a finite element (FE) formulation based on a third-order, shear-deformation beam theory. It was shown that the influence of higher-order terms is negligible on the fundamental frequencies, whereas it is significant on the frequencies of high flexural modes. Kameswara Rao et al. (2001) have studied the effect of higher-order theories on the natural frequencies of composite beams. A closed-form solution was used. Numerical examples were conducted on beams of various span-to-height ratios. The results showed that the presented theory offers significantly lower natural frequencies than those computed using the Timoshenko model in the case of thick sandwich beams. The free-vibration analysis of a composite pipe, by means of the asymptotic method, has been conducted by Yu and Hodges (2005). The differences between the generalized Timoshenko theory and classical models in computing the bending frequencies were underlined. No differences were found in the torsional frequencies. Simsek and Kocaturk (2007) have used a third-order shear-deformation theory to study free vibrations of beams with different boundary conditions. The results were compared with the Timoskenko and Euler-Bernoulli model responses. It was highlighted that higher-order models provide significantly better results than classical theories in the case of short beams and high mode numbers. A higher-order finite element model, based on the classical laminated theory, has been developed by Ganesan and Zabihollah (2007). The vibration response of laminated tapered composite beams was investigated considering the curvature as a degree of freedom of each element. This feature ensured continuous curvature and stress distribution across element interfaces, and it enhanced higher-frequency analysis capabilities. It was also shown how a higher-order formulation needs fewer elements to obtain accurate results. Kiani et al. (2009) have used different theories to investigate the prediction capability of the dynamic response of a beam subjected to a moving mass. It was shown that classical theories are unable to predict an accurate solution in the case of small slenderness ratios. Other important contributions are those by Banerjee and coworkers (Banerjee and Williams 1992, 1994; Banerjee et al. 1996; Banerjee 1998; Eslimy-Isfahany and Banerjee 2000; Banerjee and Sobey 2005) who have dealt with the free-vibration analysis and response problems of beam structures. Their analyses were based on the dynamic stiffness formulation. Nonuniform, thin-walled structures were considered as well as composite and sandwich beams. The effects of warping, shear deformation, and bending-torsion coupling on dynamic behavior were evaluated. The study of unconventional wing configurations is one of the important issues in this paper. Examples include joined wing and strut-braced configurations. Interest in these configurations is motivated by their enhanced aerodynamic properties. Some important research works that are related to joined wing structures are those by Wolkowich (1986), Frediani et al. (1999), and Demasi (2007). An interesting paper that has focused on the strut-braced configuration is by Gundlach et al. (2000).

This work presents the finite element, free-vibration analysis of several wing models by means of higher-order beam theories. Refined models are obtained within the framework of the Carrera Unified Formulation (CUF) (Carrera 2002, 2003). CUF has been developed over the last decade for plate and shell theories. It has recently been extended to beam modeling (Carrera and Giunta 2010; Carrera et al. 2010a; Carrera and Petrolo 2011). The main feature of CUF is its hierarchical formulation. In other words, the order of the model is a free-parameter (i.e., an input) of the analysis; that is, refined models are obtained with no need for ad hoc formulations. Arbitrary cross-section geometries can be modeled. Taylor-type expansions are herein exploited to define the kinematics field above the cross-section. Up to the fourth-order models are adopted. Classical models are obtained as particular examples of the general case. The finite element formulation is used to overcome the limits of closed-form solutions in dealing with arbitrary beam geometries and loading conditions. Different beam configurations are investigated. These include compact, thin-walled, conventional wing models (straight, swept, with dihedral angles, tapered), and unconventional wing models (joined wing). Isotropic materials are used. A preliminary static assessment is conducted to show the correctness of the model. The dynamic analysis is conducted by computing natural frequencies and modes. Static and dynamic results are compared with those obtained from conventional finite element models, which are based on shell and solid elements. This paper is organized as follows: a brief description of the adopted beam theories and the finite element formulation is furnished first; the main structural problems, together with the results and discussion, are then provided; finally, the main conclusions and outlook are outlined in the Conclusions section.

Preliminaries

The adopted coordinate frame is shown in Fig. 1. The beam boundaries over y are $0 \leq y \leq L$. The displacements vector is as follows:

$$\mathbf{u}(x,y,z) = \{ u_x \quad u_y \quad u_z \}^T \tag{1}$$

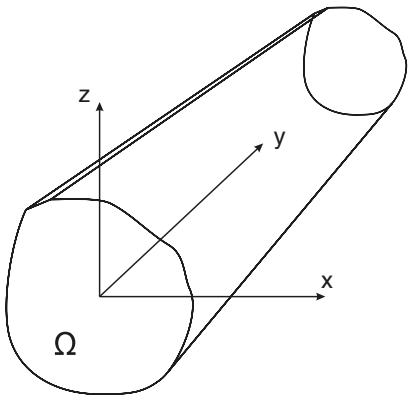

Fig. 1. Coordinate frame of the beam model

Superscript "T" represents the transposition operator. The stress, σ, and the strain, ϵ, are grouped as follows:

$$\boldsymbol{\sigma}_p = \{\, \sigma_{zz} \quad \sigma_{xx} \quad \sigma_{zx} \,\}^T, \qquad \boldsymbol{\epsilon}_p = \{\, \epsilon_{zz} \quad \epsilon_{xx} \quad \epsilon_{zx} \,\}^T$$
$$\boldsymbol{\sigma}_n = \{\, \sigma_{zy} \quad \sigma_{xy} \quad \sigma_{yy} \,\}^T, \qquad \boldsymbol{\epsilon}_n = \{\, \epsilon_{zy} \quad \epsilon_{xy} \quad \epsilon_{yy} \,\}^T \tag{2}$$

Subscript "n" stands for terms laying on the cross-section, Ω, whereas "p" stands for terms laying on planes orthogonal to Ω. Linear strain-displacement relations are used:

$$\boldsymbol{\epsilon}_p = \boldsymbol{D}_p \mathbf{u} \qquad \boldsymbol{\epsilon}_n = \boldsymbol{D}_n \mathbf{u} = (\boldsymbol{D}_{n\Omega} + \boldsymbol{D}_{ny})\mathbf{u} \tag{3}$$

with:

$$\boldsymbol{D}_p = \begin{bmatrix} 0 & 0 & \partial/\partial_z \\ \partial/\partial_x & 0 & 0 \\ \partial/\partial_z & 0 & \partial/\partial_x \end{bmatrix}, \qquad \boldsymbol{D}_{n\Omega} = \begin{bmatrix} 0 & \partial/\partial_z & 0 \\ 0 & \partial/\partial_x & 0 \\ 0 & 0 & 0 \end{bmatrix},$$
$$\boldsymbol{D}_{ny} = \begin{bmatrix} 0 & 0 & \partial/\partial_y \\ \partial/\partial_y & 0 & 0 \\ 0 & \partial/\partial_y & 0 \end{bmatrix} \tag{4}$$

Next, the Hooke's law is exploited:

$$\boldsymbol{\sigma} = \boldsymbol{C}\boldsymbol{\epsilon} \tag{5}$$

According to Eq. (2), the previous equation becomes:

$$\boldsymbol{\sigma}_p = \tilde{\boldsymbol{C}}_{pp}\boldsymbol{\epsilon}_p + \tilde{\boldsymbol{C}}_{pn}\boldsymbol{\epsilon}_n \qquad \boldsymbol{\sigma}_n = \tilde{\boldsymbol{C}}_{np}\boldsymbol{\epsilon}_p + \tilde{\boldsymbol{C}}_{nn}\boldsymbol{\epsilon}_n \tag{6}$$

In the case of isotropic material, the matrices $\tilde{\boldsymbol{C}}_{pp}$, $\tilde{\boldsymbol{C}}_{nn}$, $\tilde{\boldsymbol{C}}_{pn}$ and $\tilde{\boldsymbol{C}}_{np}$ areas follows:

$$\tilde{\boldsymbol{C}}_{pp} = \begin{bmatrix} \tilde{C}_{11} & \tilde{C}_{12} & 0 \\ \tilde{C}_{12} & \tilde{C}_{22} & 0 \\ 0 & 0 & \tilde{C}_{66} \end{bmatrix}, \qquad \tilde{\boldsymbol{C}}_{nn} = \begin{bmatrix} \tilde{C}_{55} & 0 & 0 \\ 0 & \tilde{C}_{44} & 0 \\ 0 & 0 & \tilde{C}_{33} \end{bmatrix},$$
$$\tilde{\boldsymbol{C}}_{pn} = \tilde{\boldsymbol{C}}_{np}^T = \begin{bmatrix} 0 & 0 & \tilde{C}_{13} \\ 0 & 0 & \tilde{C}_{23} \\ 0 & 0 & 0 \end{bmatrix} \tag{7}$$

For the sake of brevity, the dependence of the coefficients $[\tilde{C}]_{ij}$ versus Young's moduli and Poisson's ratio is not reported here. It can be found in Tsai (1988) or Reddy (2004).

Advanced Beam Model Based on the Unified Formulation

In the framework of the CUF (Carrera 2002, 2003; Carrera and Giunta 2010; Carrera et al. 2010a, 2011; Carrera and Petrolo 2011), the displacement field is assumed as an expansion in terms of generic functions, $F\tau$:

$$\mathbf{u} = F_\tau \mathbf{u}_\tau, \qquad \tau = 1, 2, \ldots, M \tag{8}$$

where F_τ are functions of the coordinates x and z on the cross-section. $\mathbf{u}_\tau$ is the displacement vector, and M stands for the number of terms of the expansion. According to the Einstein notation, the repeated subscript τ indicates summation. Eq. (8) consists of a Maclaurin expansion that uses as base the 2D polynomials $x^i z^j$, where i and j are positive integers. The maximum expansion order, N, is supposed to be 4. Table 1 presents M and F_τ as functions of N. For example, the second-order displacement field is as follows:

Table 1. Maclaurin's Polynomials

N	M	F_τ
0	1	$F_1 = 1$
1	3	$F_2 = xF_3 = z$
2	6	$F_4 = x^2F_5 = xzF_6 = z^2$
3	10	$F_7 = x^3F_8 = x^2zF_9 = xz^2F_{10} = z^3$
…	…	…
N	$\frac{(N+1)(N+2)}{2}$	$F_{\frac{(N^2+N+2)}{2}} = x^N F_{\frac{(N^2+N+4)}{2}} = x^{N-1}z \ldots F_{\frac{N(N+3)}{2}} = xz^{N-1}F_{\frac{(N+1)(N+2)}{2}} = z^N$

$$u_x = u_{x_1} + xu_{x_2} + zu_{x_3} + x^2u_{x_4} + xzu_{x_5} + z^2u_{x_6}$$
$$u_y = u_{y_1} + xu_{y_2} + zu_{y_3} + x^2u_{y_4} + xzu_{y_5} + z^2u_{y_6}$$
$$u_z = u_{z_1} + xu_{z_2} + zu_{z_3} + x^2u_{z_4} + xzu_{z_5} + z^2u_{z_6} \tag{9}$$

The beam model described by Eq. (9) has 18 generalized displacement variables. The in-plane linear terms, i.e., u_{x_2}, u_{x_3}, u_{z_2}, and u_{z_3}, are not present in the classical models by Euler and Timoshenko: these variables are needed to provide at least a linear distribution of twisting above the cross-section. The nine parabolic terms, i.e., $u_{x_4}, \ldots, u_{z_6}$, enhance the in-plane and out-of-plane warping capabilities of the model. Similar considerations can be found in El Fatmi and Ghazouani (2010). A more detailed description of the role played by each higher-order term can be found in Carrera and Petrolo (2011). The present unified formulation permits us to embed higher-order terms in the beam models with no need of case-dependent implementations such as the insertion of warping functions as shown in the excellent book by Novozhilov (1961). The Timoshenko beam model (TBM) can be obtained by acting on the F_τ expansion. Two conditions have to be imposed: (1) a first-order approximation kinematic field:

$$u_x = u_{x_1} + xu_{x_2} + zu_{x_3}$$
$$u_y = u_{y_1} + xu_{y_2} + zu_{y_3}$$
$$u_z = u_{z_1} + xu_{z_2} + zu_{z_3} \tag{10}$$

(2) the displacement components u_x and u_z have to be constant above the cross-section:

$$u_{x_2} = u_{z_2} = u_{x_3} = u_{z_3} = 0 \tag{11}$$

The Euler-Bernoulli beam (EBBM) can be obtained through the penalization of ϵ_{xy} and ϵ_{zy}. This condition can be imposed by using a penalty value χ in the following constitutive equations:

$$\sigma_{xy} = \chi\tilde{C}_{55}\epsilon_{xy} + \chi\tilde{C}_{45}\epsilon_{zy} \qquad \sigma_{zy} = \chi\tilde{C}_{45}\epsilon_{xy} + \chi\tilde{C}_{44}\epsilon_{zy} \tag{12}$$

The classical theories and the first-order models require the assumption of opportunely reduced material stiffness coefficients to correct Poisson's locking [see Carrera and Brischetto (2008)]. Unless differently specified, for classical and first-order models Poisson's locking is corrected according to Carrera and Giunta (2010). Introducing the shape functions, N_i, and the nodal displacement vector, $\mathbf{q}_{\tau i}$:

$$\mathbf{q} = \{\, q_{u_{x_{\tau i}}} \quad q_{u_{y_{\tau i}}} \quad q_{u_{z_{\tau i}}} \,\}^T \tag{13}$$

The displacement vector becomes:

$$\mathbf{u} = N_i F_\tau \mathbf{q}_{\tau i} \tag{14}$$

For the sake of brevity, the shape functions are not reported here. They can be found in many books, for instance in Bathe (1996). Elements with four nodes (B4) are formulated; that is, a cubic approximation along the y axis is adopted. It has to be highlighted that, although the order of the beam model is related to the expansion on the cross-section, the number of nodes per each element is related to the approximation along the longitudinal axis. These two parameters are totally free and not related to each others. An N-order beam model is therefore a theory that exploits an N-order polynomial to describe the kinematics of the cross-section. The stiffness matrix of the elements and the external loadings, which are consistent with the model, are obtained via the Principle of Virtual Displacements:

$$\delta L_{\text{int}} = \int_V (\delta \boldsymbol{\epsilon}_p^T \boldsymbol{\sigma}_p + \delta \boldsymbol{\epsilon}_n^T \boldsymbol{\sigma}_n) dV = \delta L_{\text{ext}} \tag{15}$$

where L_{int} stands for the strain energy, and L_{ext} is the work of the external loadings. δ stands for the virtual variation. The virtual variation of the strain energy is rewritten using Eqs. (3), (6), and (14), and in a compact format it becomes:

$$\delta L_{\text{int}} = \delta \mathbf{q}_{\tau i}^T \mathbf{K}^{ij\tau s} \mathbf{q}_{sj} \tag{16}$$

where $\mathbf{K}^{ij\tau s}$ is the stiffness matrix in the form of the fundamental nucleus. Its components are as follows:

$$\begin{aligned}
K_{xx}^{ij\tau s} &= \tilde{C}_{22} \int_\Omega F_{\tau,x} F_{s,x} d\Omega \int_l N_i N_j dy + \tilde{C}_{66} \int_\Omega F_{\tau,z} F_{s,z} d\Omega \int_l N_i N_j dy + \tilde{C}_{44} \int_\Omega F_\tau F_s d\Omega \int_l N_{i,y} N_{j,y} dy \\
K_{xy}^{ij\tau s} &= \tilde{C}_{23} \int_\Omega F_{\tau,x} F_s d\Omega \int_l N_i N_{j,y} dy + \tilde{C}_{44} \int_\Omega F_\tau F_{s,x} d\Omega \int_l N_{i,y} N_j dy \\
K_{xz}^{ij\tau s} &= \tilde{C}_{12} \int_\Omega F_{\tau,x} F_{s,z} d\Omega \int_l N_i N_j dy + \tilde{C}_{66} \int_\Omega F_{\tau,z} F_{s,x} d\Omega \int_l N_i N_j dy \\
K_{yx}^{ij\tau s} &= \tilde{C}_{44} \int_\Omega F_{\tau,x} F_s d\Omega \int_l N_i N_{j,y} dy + \tilde{C}_{23} \int_\Omega F_\tau F_{s,x} d\Omega \int_l N_{i,y} N_j dy \\
K_{yy}^{ij\tau s} &= \tilde{C}_{55} \int_\Omega F_{\tau,z} F_{s,z} d\Omega \int_l N_i N_j dy + \tilde{C}_{44} \int_\Omega F_{\tau,x} F_{s,x} d\Omega \int_l N_i N_j dy + \tilde{C}_{33} \int_\Omega F_\tau F_s d\Omega \int_l N_{i,y} N_{j,y} dy \\
K_{yz}^{ij\tau s} &= \tilde{C}_{55} \int_\Omega F_{\tau,z} F_s d\Omega \int_l N_i N_{j,y} dy + \tilde{C}_{13} \int_\Omega F_\tau F_{s,z} d\Omega \int_l N_{i,y} N_j dy \\
K_{zx}^{ij\tau s} &= \tilde{C}_{12} \int_\Omega F_{\tau,z} F_{s,x} d\Omega \int_l N_i N_j dy + \tilde{C}_{66} \int_\Omega F_{\tau,x} F_{s,z} d\Omega \int_l N_i N_j dy \\
K_{zy}^{ij\tau s} &= \tilde{C}_{13} \int_\Omega F_{\tau,z} F_s d\Omega \int_l N_i N_{j,y} dy + \tilde{C}_{55} \int_\Omega F_\tau F_{s,z} d\Omega \int_l N_{i,y} N_j dy \\
K_{zz}^{ij\tau s} &= \tilde{C}_{11} \int_\Omega F_{\tau,z} F_{s,z} d\Omega \int_l N_i N_j dy + \tilde{C}_{66} \int_\Omega F_{\tau,x} F_{s,x} d\Omega \int_l N_i N_j dy + \tilde{C}_{55} \int_\Omega F_\tau F_s d\Omega \int_l N_{i,y} N_{j,y} dy
\end{aligned} \tag{17}$$

The virtual variation of the work of the inertial loadings is as follows:

$$\delta L_{ine} = \int_V \rho \ddot{u} \delta u^T dV \tag{18}$$

where ρ stands for the density of the material, and $\ddot{u}$ is the acceleration vector. Eq. (18) is rewritten using Eqs. (3) and (14):

$$\delta L_{ine} = \int_l \delta q_{\tau i}^T N_i \left[\int_\Omega \rho (F_\tau \mathbf{I})(F_s \mathbf{I}) d\Omega \right] N_j \ddot{q}_{sj} dy \tag{19}$$

where $\ddot{q}$ is the nodal acceleration vector. The last equation can be rewritten in the following compact manner:

$$\delta L_{\text{ine}} = \delta q_{\tau i}^T \mathbf{M}^{\text{ij}\tau s} \ddot{q}_{sj} \tag{20}$$

where $\mathbf{M}^{ij\tau s}$ is the mass matrix in the form of the fundamental nucleus. Its components are:

$$\begin{aligned}
M_{xx}^{ij\tau s} &= M_{yy}^{ij\tau s} = M_{zz}^{ij\tau s} = \rho \int_\Omega F_\tau F_s d\Omega \int_l N_i N_j dy \\
M_{xy}^{ij\tau s} &= M_{xz}^{ij\tau s} = M_{yx}^{ij\tau s} = M_{yz}^{ij\tau s} = M_{zx}^{ij\tau s} = M_{zy}^{ij\tau s} = 0
\end{aligned} \tag{21}$$

It should be noted that no assumptions on the approximation order have been done. It is therefore possible to obtain refined beam models without changing the formal expression of the nucleus components. This is the key point of CUF, which permits, with only nine FORTRAN statements, to implement any-order beam theories. The shear locking is corrected through the selective integration [see Bathe (1996)]. The undamped dynamic problem can be written as it follows:

$$\boldsymbol{M}\,\ddot{a} + \boldsymbol{K} a = \mathbf{p} \tag{22}$$

where a is the vector of the nodal unknowns and p is the loadings vector. With the introduction of harmonic solutions, it is possible to compute the natural frequencies, ω_i, for the homogenous case, by solving an eigenvalues problem:

$$(-\omega_i^2 \mathbf{M} + \mathbf{K}) a_i = 0 \tag{23}$$

where a_i is the i-th eigenvector. Generally oriented structures have to be analyzed in the outlook of aeroelastic applications. The finite element matrices are computed with respect to an arbitrary oriented local reference system. The relation that furnishes the global coordinated of the local reference system is as follows:

$$\mathbf{i}^{\text{loc}} = e_{11}^{\text{loc}}\mathbf{i} + e_{12}^{\text{loc}}\mathbf{j} + e_{13}^{\text{loc}}\mathbf{k} \qquad \mathbf{j}^{\text{loc}} = \mathbf{e}_{21}^{\text{loc}}\mathbf{i} + \mathbf{e}_{22}^{\text{loc}}\mathbf{j} + \mathbf{e}_{23}^{\text{loc}}\mathbf{k}$$
$$\mathbf{k}^{\text{loc}} = \mathbf{e}_{31}^{\text{loc}}\mathbf{i} + \mathbf{e}_{32}^{\text{loc}}\mathbf{j} + \mathbf{e}_{33}^{\text{loc}}\mathbf{k} \tag{24}$$

where **i**, **j**, and **k** are the unit vectors of the global reference system; $\mathbf{i}^{\text{loc}}$, $\mathbf{j}^{\text{loc}}$, $\mathbf{k}^{\text{loc}}$ are the unit vectors of the local reference system; and the nine coefficients $e_{11}^{\text{loc}}, ..., e_{33}^{\text{loc}}$ are the global coordinates of the local unit vectors. They are grouped in the matrix e^{loc}. The finite element matrices in the global reference system are given by:

$$\mathbf{K}^{ij\tau s} = \mathrm{e}^{\text{loc}^{\mathrm{T}}}\,\mathbf{K}_{\text{loc}}^{ij\tau s}\,\mathrm{e}^{\text{loc}} \tag{25}$$

$$\mathbf{M}^{ij\tau s} = \mathrm{e}^{\text{loc}^{\mathrm{T}}}\,\mathbf{M}_{\text{loc}}^{ij\tau s}\,\mathrm{e}^{\text{loc}} \tag{26}$$

Results and Discussion

A free-vibration analysis of different beam models is conducted in this section. An isotropic material is used. Young's modulus, E, is equal to 75 [GPa]. The Poisson ratio, ν, is equal to 0.33. The density of the material, ρ, is equal to 2,700 [kg/m^3]. Beams geometries are described in the following sections.

Solid Rectangular Cross-Section Beam

A rectangular compact beam is considered as a first example to assess the proposed FE model. The coordinate frame and the cross-section geometry are shown in Fig. 2. The span-to-height ratio, L/h, is equal to 100. The straight and the swept beams have square cross-sections with b equal to 0.2 m. Fig. 3 shows the notation used to deal with the swept configuration. The case considered has h_Λ equal to 5 m, this choice makes the sweep angle, Λ, equal to 14.3°. The swept-tapered beam keeps this angle, whereas b varies linearly along the spanwise direction, y. The clamped section is square with $b = 0.2$ m and the free-tip section is rectangular with b equal to 0.1 m, and h equal to 0.2 m. A static analysis of a cantilever is first performed to evaluate the convergence properties of the finite element mesh. Four-node elements are used (B4). A vertical force is applied at the center of the free-tip cross-section, [$b/2$, L, 0]. The vertical displacement, u_z, is evaluated at [0, L, 0]. An MSC Nastran model made of solid elements is used as a reference solution. The computed results are presented in Table 2. The free-vibration analysis is also considered. The first five bending modes are analyzed. The natural frequencies, f_i, are compared with those obtained by the EBBM:

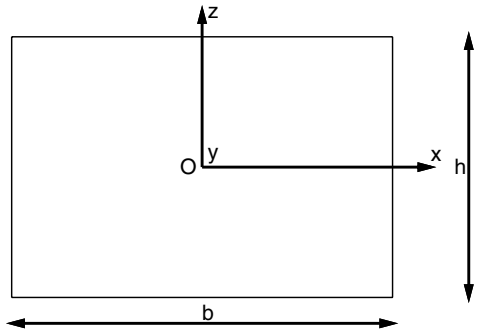

Fig. 2. Rectangular cross-section

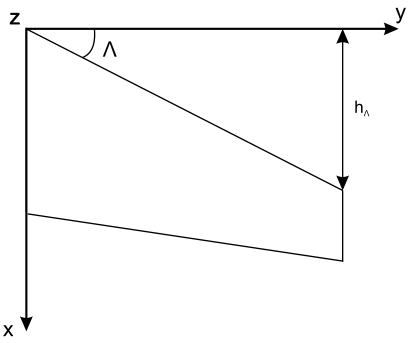

Fig. 3. Graphical definition of the sweep angle, Λ

Table 2. Vertical Displacement, $u_z \times 10^{-2}$ m, for Different Beam Models and Meshes. Rectangular Cross-Section Cantilever Beam

Number of elements	EBBM	TBM	$n = 1$	$n = 2$	$n = 3$	$n = 4$
Straight beam			−1.332[a]			
10	−1.333	−1.333	−1.333	−1.324	−1.324	−1.324
20	−1.333	−1.333	−1.333	−1.328	−1.329	−1.329
30	−1.333	−1.333	−1.333	−1.330	−1.330	−1.330
Swept beam			−1.507[a]			
10	−1.515	−1.515	−1.515	−1.504	−1.504	−1.504
20	−1.515	−1.515	−1.515	−1.510	−1.510	−1.510
30	−1.515	−1.515	−1.515	−1.510	−1.510	−1.510
Swept-tapered beam			−1.753[a]			
10	−1.755	−1.755	−1.755	−1.744	−1.744	−1.744
20	−1.753	−1.753	−1.753	−1.748	−1.748	−1.748
30	−1.753	−1.753	−1.753	−1.749	−1.749	−1.749

[a]Computed with MSC Nastran, solid elements.

$$f_i = \frac{1}{2\pi}\left(\frac{(\lambda_i L)^2}{L^2}\left(\frac{EI}{\rho A}\right)^{\frac{1}{2}}\right) \tag{27}$$

For the sake of brevity, the values of $\lambda_i L$ are not reported here. They can be found in Craig (1981) or Mcconnell (1995). Table 3 shows

Table 3. First Four Bending Frequencies, Hz, for Different Beam Models and Meshes. Cantilever Straight Beam with Rectangular Cross-Section

Number of elements	EBBM	TBM	$N = 1$	$N = 2$	$N = 3$	$N = 4$
f_1			0.426[a]			
10	0.428	0.426	0.426	0.428	0.428	0.428
20	0.426	0.426	0.426	0.427	0.427	0.427
30	0.426	0.426	0.426	0.426	0.426	0.426
f_2			2.668[a]			
10	2.668	2.667	2.667	2.680	2.679	2.679
20	2.668	2.667	2.667	2.673	2.673	2.673
30	2.668	2.667	2.667	2.671	2.671	2.671
f_3			7.470[a]			
10	7.468	7.461	7.461	7.498	7.497	7.497
20	7.468	7.461	7.461	7.480	7.479	7.479
30	7.468	7.461	7.461	7.474	7.473	7.473
f_4			14.639[a]			
10	14.630	14.607	14.607	14.680	14.676	14.676
20	14.630	14.607	14.607	14.644	14.639	14.639
30	14.630	14.607	14.607	14.632	14.628	14.628

[a]Reference value computed by means of Eq. (27).

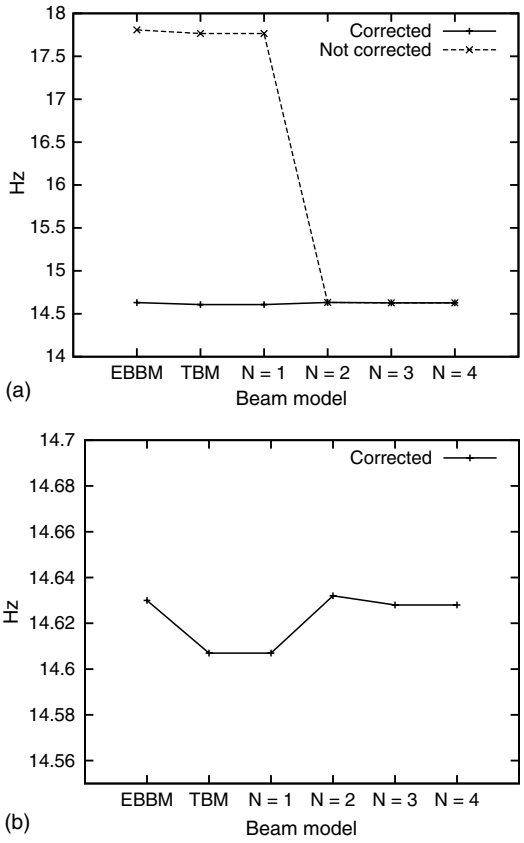

Fig. 4. Effect of the Poisson locking correction on the fourth bending frequency of the straight beam with rectangular cross-section (a) with and without correction (b) with correction

the first four bending frequencies in the case of a cantilever straight beam for different models and meshes. Fig. 4 presents the fourth bending frequency values obtained with and without the Poisson locking correction for the EBBM, TBM, and full linear models. Table 4 shows the first four bending frequencies of a fixed-pinned straight beam, and values from Eq. (27) are used as references. The cantilever swept and swept-tapered beam models are addressed in Tables 5 and 6, respectively. The first three bending frequencies along the x- and z-directions are reported. An MSC Nastran solid model is used as a benchmark. Solid elements with an almost unitary aspect ratio have been used. The first row reports the total number of degrees of freedom (DOF) of the considered models, that is, the computational cost of each analysis. The static analysis

Table 4. First Four Bending Frequencies, Hz, for Different Beam Models and Meshes. Fixed-Pinned Straight Beam with Rectangular Cross-Section, 30 B4 Mesh

EBBM	TBM	$N=1$	$N=2$	$N=3$	$N=4$	Nastran (solid)
f_1				1.866[a]		
1.867	1.866	1.866	1.869	1.869	1.869	1.868
f_2				6.050[a]		
6.048	6.044	6.044	6.054	6.053	6.053	6.049
f_3				12.621[a]		
12.617	12.598	12.598	12.620	12.617	12.617	12.609
f_4				21.584[a]		
21.570	21.518	21.518	21.556	21.546	21.546	21.535

[a]Reference value computed by means of Eq. (27).

Table 5. First Three Bending Frequencies, Hz, in the x-and z-Directions. Cantilever Swept Rectangular Beam, 30 B4 Mesh

Model type	EBBM	TBM	$N=1$	$N=2$	$N=3$	$N=4$	Nastran (solid)
Number of DOF	273	455	819	1,638	2,730	4,095	5,565
				x-direction			
f_1	0.388	0.387	0.387	0.388	0.388	0.388	0.389
f_2	2.427	2.426	2.426	2.430	2.430	2.430	2.437
f_3	6.795	6.789	6.789	6.801	6.800	6.800	6.819
				z-direction			
f_1	0.400	0.400	0.400	0.400	0.400	0.400	0.400
f_2	2.505	2.504	2.504	2.508	2.508	2.508	2.507
f_3	7.012	7.006	7.006	7.018	7.017	7.017	7.014

Table 6. First Three Bending Frequencies, Hz, in the x-and z-Directions. Cantilever Swept-Tapered Rectangular Beam, 30 B4 Mesh

Model type	EBBM	TBM	$N=1$	$N=2$	$N=3$	$N=4$	Nastran (solid)
Number of DOF	273	455	819	1,638	2,730	4,095	5,565
				x-direction			
f_1	0.430	0.422	0.422	0.422	0.422	0.422	0.427
f_2	2.020	2.018	2.018	2.021	2.021	2.021	2.046
f_3	5.207	5.205	5.205	5.212	5.212	5.212	5.279
				z-direction			
f_1	0.499	0.491	0.491	0.491	0.491	0.491	0.490
f_2	2.675	2.672	2.672	2.677	2.676	2.676	2.668
f_3	7.181	7.175	7.175	7.187	7.186	7.186	7.165

of the compact, rectangular, slender beam suggests the following conclusions.

1. In all the considered beam configurations, the linear models, $N < 2$, furnishes the largest displacement values. This result is because of the Poisson locking correction that is just activated for the linear cases, and it is coherent with Carrera et al. (2010a).
2. No significant differences have been observed among the classical models, EBBM and TBM, and the full linear case; that is, the shear effect and the linear terms of the cross-section displacements have not had remarkable effects in this case. This is due to the fact that the beam is slender, $L/h = 100$, the section is compact, and a bending load is applied.
3. The results are in good agreement with those furnished by the solid elements.
4. As far as the mesh refinement is concerned, the use of 30 four-node elements offers appreciable convergent capabilities.
5. The good match between the results given by the present beam formulation and MSC Nastran is confirmed, even in the cases

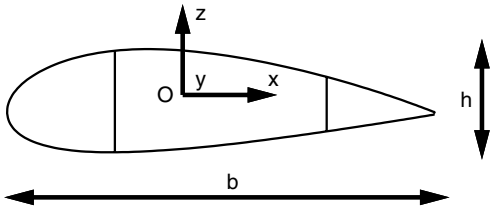

Fig. 5. Wing cross-section

of swept and swept-tapered beam configurations. This aspect offers validation of the adopted formulation. As far as the free-vibration analysis is concerned, the following conclusions hold.

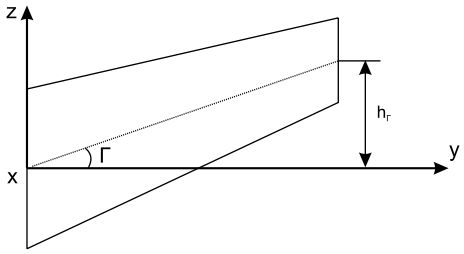

Fig. 6. Graphical definition of the dihedral angle, Γ

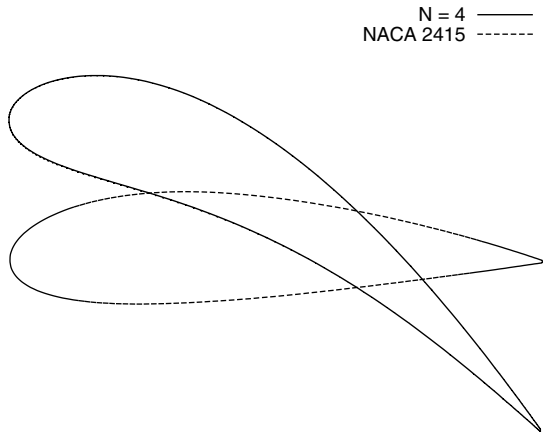

Fig. 7. Wing cross-section 17th natural modal shape, $f = 604$ Hz, straight wing model

Table 7. Bending Natural Frequencies, *Hz*, of the Cantilever Wing Models for Different Theories, 10 B4 Mesh

Model type	EBBM	TBM	$N = 1$	$N = 2$	$N = 3$	$N = 4$	Nastran (solid)
Number of DOF	93	155	279	558	930	1,395	> 6,000,000
				Straight			
f_1, bending z-dir	5.872	5.866	5.866	5.984	5.934	5.925	5.864
f_2, bending x-dir	33.340	32.709	32.709	32.891	32.712	32.696	32.335
f_3, bending z-dir	36.735	36.581	36.581	37.206	36.447	36.288	34.844
f_4, bending z-dir	102.634	101.617	101.617	103.430	99.100	98.318	81.976
				Sweep + dihedral			
f_1, bending z-dir	4.126	4.128	4.128	4.200	4.171	4.166	4.114
f_2, bending x-dir	23.736	23.432	23.432	23.560	23.472	23.465	23.778
f_3, bending z-dir	25.854	25.782	25.783	26.189	25.798	25.722	24.991
f_4, bending z-dir	72.288	71.815	71.815	73.035	70.837	70.459	64.731

Note: dir, direction.

Table 8. Bending Natural Frequencies, Hz, of the Cantilever Wing Models for Different Theories, 30 B4 Mesh

Model type	EBBM	TBM	$N = 1$	$N = 2$	$N = 3$	$N = 4$	Nastran (solid)
Number of DOF	273	455	819	1,638	2,730	4,095	> 6,000,000
				Straight			
f_1, bending z-dir	5.872	5.866	5.866	5.972	5.922	5.913	5.864
f_2, bending x-dir	33.340	32.709	32.709	32.834	32.656	32.625	32.335
f_3, bending z-dir	36.735	36.581	36.581	37.127	36.376	36.216	34.844
f_4, bending z-dir	102.634	101.617	101.617	103.210	98.918	98.133	81.976
				Sweep + dihedral			
f_1, bending z-dir	4.126	4.128	4.128	4.191	4.162	4.157	4.114
f_2, bending x-dir	23.736	23.432	23.432	23.513	23.426	23.411	23.778
f_3, bending z-dir	25.854	25.782	25.783	26.132	25.746	25.668	24.991
f_4, bending z-dir	72.288	71.815	71.815	72.866	70.696	70.317	64.731

Note: dir, direction.

Table 9. First Torsional Natural Frequency, Hz, of the Cantilever Wing models for Different Theories, 30 B4 Mesh

Model type	EBBM	TBM	$N = 1$	$N = 2$	$N = 3$	$N = 4$	Nastran (solid)
Number of DOF	273	455	819	1,638	2,730	4,095	> 6,000,000[a]
Straight	—[a]	—[a]	161.581	56.857	54.457	53.979	44.481
Sweep + dihedral	—[a]	—[a]	—[b]	48.689	46.692	46.304	39.443

[a]No torsional modes are provided by this model.
[b]No torsional modes have been found for frequencies up to 200 Hz.

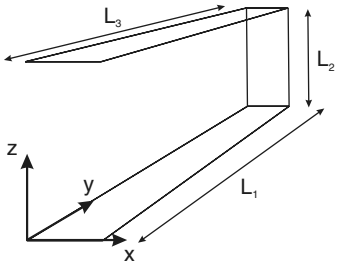

Fig. 8. Joined-wing scheme, the horizontal segments are both clamped at $y = 0$

1. The results match those obtained with the analytical model. As seen for the static case, the Poisson locking correction greatly enhances the flexibility of the finite element model for EBBM, TBM, and full linear models. Note that this correction can lead to lower frequencies than those from higher-order models. This result agrees with that of Carrera et al. (2010a, 2011).
2. The free-vibration analysis highlights the difference between the EBBM solution and the TBM one. The higher the mode number, the larger the differences. No very significant differences were observed between TBM and the full linear case.
3. A 10-element mesh furnishes the first natural frequency with an appreciable accuracy. However, the higher the mode number, the larger the influence of a finer mesh. Because the 30-element mesh offers good convergent behavior, it will be used for all the subsequent analyses.
4. The results show a good match with those obtained with the solid model. This confirms the validity of the adopted formulation in dealing with arbitrary oriented structures (swept) with varying cross-section geometries along the longitudinal axis (tapered).
5. The higher the order of the beam model, the larger the total number of DOF. A fourth-order model requires a similar total number of DOF to that of the solid model because b/h is close to unity and the cross-section is compact.

Airfoil-Shaped Beam

A cantilever arbitrary-shaped, thin-walled beam is considered in this section. The cross-section contour is defined by the NACA 2415 airfoil profile. The cross-section geometry is shown in Fig. 5. The chord length, b, is assumed equal to 1 m. A three-cell section is evaluated. The cells are obtained by inserting two beams along the spanwise direction at 25% and 75% of the chord. The span-to-chord ratio, L/b, is assumed to be equal to 5; that is, a moderately short structure is considered. The graphical definitions of the sweep and dihedral angles are shown in Figs. 3 and 6. Two different configurations are considered: a straight wing, i.e., $h_{\Delta,}$ $h_\Gamma = 0$, and a wing with both sweep and dihedral angle. In this latter case, h_Δ and h_Γ are equal to 2 m, i.e., $\Delta = 21.8^\circ$ and $\Gamma = 21.8^\circ$. An Ansys solid model is adopted for result comparison purposes. Tables 7 and 8 show the first four bending frequencies for the two considered wing configurations, 10 B4 and 30 B4 meshes are used, respectively. The first torsional frequency is shown in Table 9. Fig. 7 shows the cross-section modal shape of the free-tip obtained via a fourth-order model with a significant distortion of the airfoil contour. The following considerations can be made.

1. A good match is found with the reference solutions.
2. The bending modes can be detected using classical models. However, the importance of higher-order terms increases for higher vibration modes.
3. The investigation of the torsional modes underlines the importance of the refined models. At least a second-order theory is needed to obtain a reliable estimation of the torsional frequency. In the presence of sweep and dihedral angles, the ineffectiveness of linear models is even more evident. It has to be highlighted that, although EBBM and TBM cannot provide torsional modes, the $N = 1$ model is able to detect the torsion of the cross-section; however, higher-order terms are needed to compute more accurate torsional frequencies. This aspect is consistent to what is presented in Carrera et al. (2010a) for the static case.
4. The influence of the higher-order terms is more relevant on the torsional modes than on the bending ones.

Table 10. Natural Frequencies, *Hz*, of the Joined Rectangular Wing for Different Beam Models and Comparison with Those obtained via Shell Elements in Nastran

Model type	EBBM	TBM	$N = 1$	$N = 2$	$N = 3$	$N = 4$	Nastran (shell)
Number of DOF	408	680	1,224	2,448	4,080	6,120	4,242
				Bending z-direction			
f_1	1.203	1.152	1.148	1.175	1.164	1.162	1.116
f_2	5.417	5.414	5.373	5.532	5.466	5.454	4.620
f_3	6.620	6.613	6.575	6.760	6.680	6.667	6.287
f_4	14.929	14.911	14.798	15.260	15.052	15.022	13.110
f_5	16.571	16.553	16.450	16.961	16.725	16.693	15.738
				Bending x-direction			
f_1	11.510	11.361	7.913	7.933	7.882	7.875	6.682
f_2	65.600	62.511	46.150	46.296	45.965	45.941	43.112
				Torsional			
f_1	—[a]	—[a]	—[b]	33.774	33.548	33.177	31.417
f_2	—[a]	—[a]	—[b]	34.034	33.803	33.442	31.658
				Others			
f_1	119.290	107.005	56.101	47.803	47.553	47.512	47.118

[a]No torsional modes are provided by this model.
[b]No torsional modes have been found for frequencies up to 200 Hz.

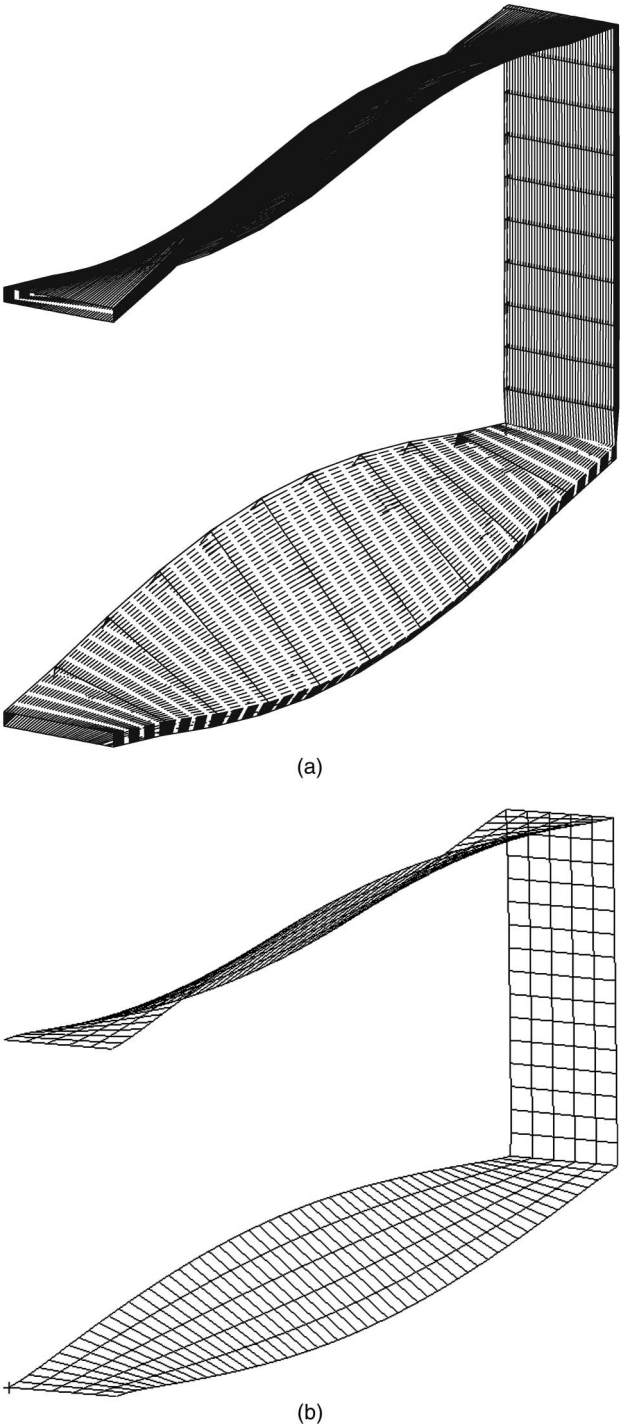

Fig. 9. Comparison between the present beam and the Nastran solution of a torsional mode of the joined-wing: (a) present Beam, $f = 33.216$ Hz; (b) nastran, $f = 31.417$ Hz

5. Refined models are able to detect the distortion of the cross-section. It is noteworthy that this aspect is particular relevant when thin-walled structures are considered.
6. The TBM and the full linear models provide the same results for bending modes.
7. The combined presence of the sweep and dihedral angles does not corrupt the accuracy of the solution.
8. The difference in computational cost between the beam and the solid models is more evident in the case of a thin-walled structure than for the compact one of the previous section.

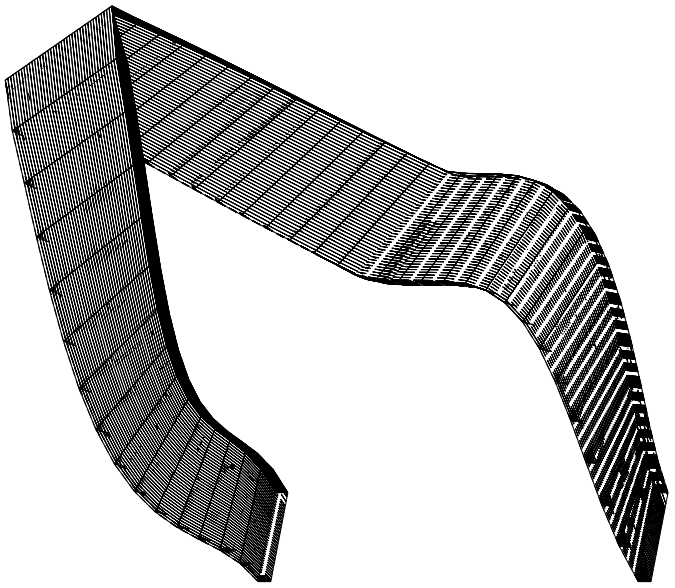

Fig. 10. Differential bending mode of the rectangular joined wing. $f = 47.512$ Hz

Table 11. Natural Frequencies, *Hz*, of the Joined Wing with the Airfoil-shaped Cross-Section

Model type	EBBM	TBM	$N = 1$	$N = 2$	$N = 3$	$N = 4$
Number of DOF	408	680	1,224	2,448	4,080	6,120
			Bending z-direction			
f_1	1.735	1.728	1.717	1.747	1.739	1.736
f_2	8.125	8.115	8.010	8.193	8.135	8.118
f_3	9.923	9.912	9.817	10.024	9.957	9.939
f_4	22.384	22.324	22.043	22.566	22.384	22.337
f_5	24.850	24.786	24.530	25.100	24.898	24.850
			Bending x-direction			
f_1	11.511	11.361	8.148	8.158	8.089	8.080
f_2	65.600	62.511	46.827	46.918	46.528	46.476
			Torsional			
f_1	—[a]	—	152.689	49.721	49.409	48.375
f_2	—	—	162.443	52.803	52.476	52.722
			Others			
f_1	119.291	107.005	56.488	45.982	45.722	45.338

[a]No torsional modes are provided by this model.

9. A fourth-order model cannot be enough to detect the exact torsional frequency or higher bending modes. This issue is typical of thin-walled structures as clearly shown in Carrera et al. (2010b), where $N = 11$ models were used to detect the right distortion of a thin-walled cylinder loaded by a point force.

Joined Wing

A joined wing model is considered as the last assessment of the present beam formulation. The geometry of the wing is shown in Fig. 8. The structure is composed of three segments: two horizontal and one vertical. As far as the boundary conditions are considered, the horizontal segments are both clamped at $y = 0$. Two cross-section geometries are considered: rectangular and airfoil-shaped. A compact rectangular cross-section is first considered, as shown in Fig. 2. The height, h, is equal to 0.1 m and the width,

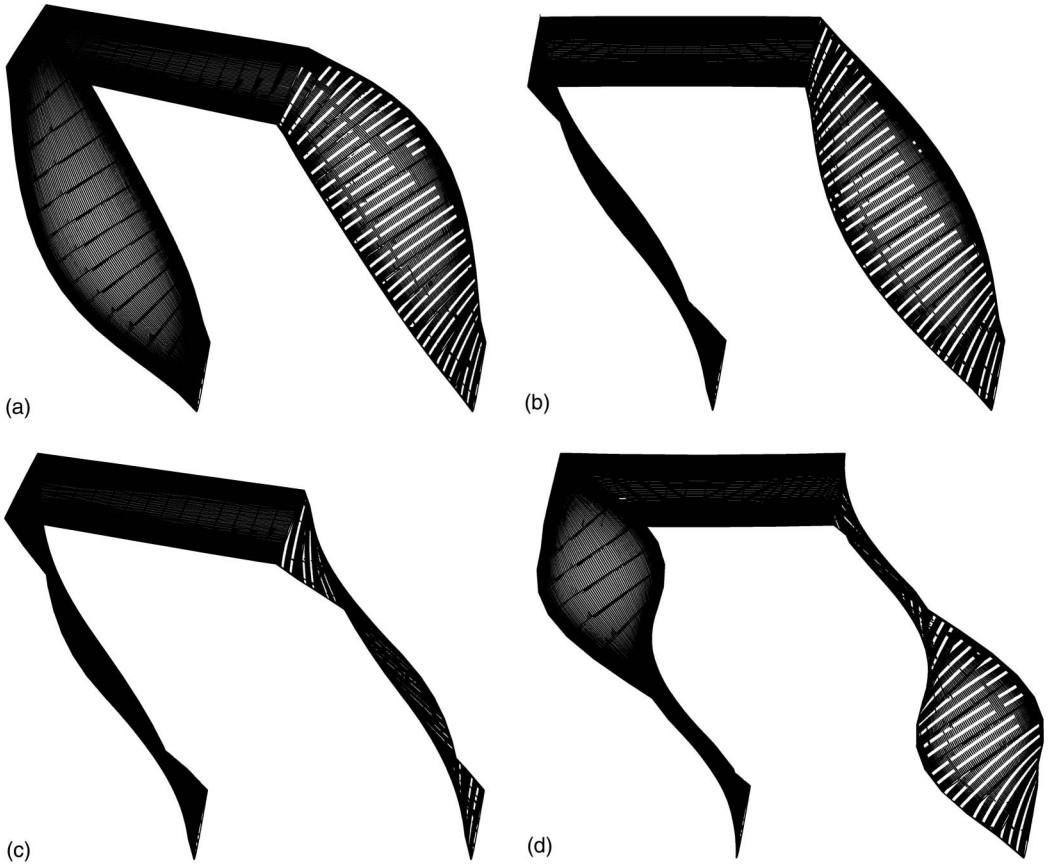

Fig. 11. Various modal shapes of the joined-wing with airfoil-shaped cross-section: (a) $f = 45.892$ Hz; (b) $f = 49.721$ Hz; (c) $f = 52.803$ Hz; (d) $f = 100.364$ Hz

b, is equal to 1 m. The horizontal segments have L_1/h and L_3/h equal to 100, whereas for the vertical segment, L_2/h is equal to 30. Forty-five four-node beam elements are used as the mesh. An MSC Nastran shell model is used to compare the results. The different types of natural frequencies are reported in Table 10. A torsional mode shape is shown in Fig. 9. The last row in Table 10 is related to a particular mode shape characterized by a differential bending of the horizontal segments, which induces a torsion of the vertical part. This mode is shown in Fig. 10. The second joined wing model has the airfoil-shaped cross-section, as shown in Fig. 5. The horizontal segments have L_1/b and L_3/b equal to 10, whereas for the vertical segment, L_2/b is equal to 3. Some natural frequencies are reported in Table 11. Some modal shapes are reported in Fig. 11. The following remarks can be made.

1. In the case of a rectangular cross-section, the total number of degrees of freedom is lower than that of the shell model in the cases of linear and parabolic beam models. In the case of cubic expansion, the number of DOF's is almost the same, whereas the fourth-order model requires a larger number of displacement variables than the shell model. This is because a compact rectangular cross-section is considered. It should be pointed out that the analysis of the airfoil-shaped cross-section requires the same amount of DOF's as the compact rectangular one, whereas modeling via shell elements would probably need a considerably larger effort.
2. The results are in good agreement with those furnished by the shell model.
3. It has been confirmed that the torsional modes are detected by higher-order models than the linear ones.
4. The proper detection of the torsional modes as well as of the differential bending ones shows that the present beam model is able to detect complex modal deformed configurations that are usually furnished by shell models. This kind of result is therefore referred to as shell-like.
5. The x-direction bending frequencies by TBM and EBBM present larger differences with respect to the refined models than the z-direction ones. This is most likely because such a bending mode makes the vertical portion of the joined wing rotate along its local longitudinal axis, and this rotation cannot be properly detected by TBM and EBBM because no in-plane distortions are foreseen by these models.

Conclusions

The free-vibration analysis of classical and joined wings, based on higher-order beam theories, has been presented in this paper. CUF has been used for the systemic implementation of refined models. According to CUF, the element stiffness and mass matrices are obtained in a compact form, named fundamental nucleus, that does not depend on the theory approximation order; that is, the order of the model is assumed as a free-parameter of the modeling. Elements based on classical theories have been derived as particular cases. A preliminary static analysis has been conducted to validate the present formulation in comparison with 3D solid element models. The analysis conducted has shown an excellent match between the models. The numerical analysis has been conducted for the investigation of dynamic behavior in terms of natural frequencies and vibration modes. Comparisons with shell and solid wing models of commercial FE codes have been made. The following main

conclusions can be drawn. The built beam formulation permits us to deal in an unified manner with the following:

1. Arbitrary cross-sections geometries;
2. Compact and thin-walled structures;
3. Straight as well as arbitrary orientated structures; and
4. Unconventional joined wing configurations.

The use of higher-order theories has permitted classical beam model limitations to be overcome. The comparison with shell and solid models has shown the shell capabilities of the refined beam theories; that is, accurate modal shapes for thin-walled structures can be obtained by means of significantly less cumbersome 1D elements. Furthermore, the effects of the higher-order terms become significant when:

1. Thin-walled cross-section geometries are adopted;
2. The beam is not slender; and
3. The aim of the structural dynamics analysis is the proper prediction of vibration modes such as torsional ones.

The use of the proposed beam models appears suitable for aeroelastic applications that include airfoil in-plane deformations, and for extensions to wings made of advanced composite materials. These topics could be the subject of future work.

Acknowledgments

The financial support from the Regione Piemonte project MICRO-COST is gratefully acknowledged.

References

Banerjee, J. R. (1998). "Free vibration of axially loaded composite Timoshenko beams using the dynamic stiffness matrix method." *Comput. Struct.*, 69(2), 197–208.

Banerjee, J. R., and Sobey, A. J. (2005). "Dynamic stiffness formulation and free vibration analysis of a three-layered sandwich beam." *Int. J. Solids Struct.*, 42(8), 2181–2197.

Banerjee, J. R., and Williams, F. W. (1992). "Coupled bending-torsional dynamic stiffness matrix for Timoshenko beam elements." *Comput. Struct.*, 42(3), 301–310.

Banerjee, J. R., and Williams, F. W. (1994). "Clamped-clamped natural frequencies of a bending-torsion coupled beam." *J. Sound Vib.*, 176(3), 301–306.

Banerjee, J. R., Guo, S., and Howson, W. P. (1996). "Exact dynamic stiffness matrix of a bending-torsion coupled beam including warping." *Comput. Struct.*, 59(4), 613–621.

Bathe, K. (1996). *Finite element procedure*, Prentice Hall, Upper Saddle River.

Bishop, R. E. D., Cannon, S. M., and Miao, S. (1989). "On coupled bending torsional vibration of uniform beams." *J. Sound Vib.*, 131(3), 457–464.

Carrera, E. (2002). "Theories and finite elements for multilayered, anisotropic, composite plates and shells." *Arch. Comput. Methods Eng.*, 9(2), 87–140.

Carrera, E. (2003). "Theories and finite elements for multilayered plates and shells: A unified compact formulation with numerical assessment and benchmarking." *Arch. Comput. Methods Eng.*, 10(3), 215–296.

Carrera, E., and Brischetto, S. (2008). "Analysis of thickness locking in classical, refined and mixed multilayered plate theories." *Compos. Struct.*, 82(4), 549–562.

Carrera, E., and Giunta, G. (2010). "Refined beam theories based on a unified formulation." *Int. J. Appl. Mech. Eng.*, 2(1), 117–143.

Carrera, E., and Petrolo, M. (2011). "On the effectiveness of higher-order terms in refined beam theories." *J. Appl. Mech.*, 78(2). 10.1115/1.4002207.

Carrera, E., Giunta, G., Nali, P., and Petrolo, M. (2010a). "Refined beam elements with arbitrary cross-section geometries." *Comput. Struct.*, 88 (5–6), 283–293, 10.1016/j.compstruc.2009.11.002.

Carrera, E., Petrolo, M., and Nali, P. (2011). "Unified formulation applied to free vibrations finite element analysis of beams with arbitrary section." *Shock Vib.*, 18(3), 485–502.

Carrera, E., Giunta, G., and Petrolo, M. (2010b). "A modern and compact way to formulate classical and advanced beam theories." Chapter 4, *Developments in computational structures technology*, B. H. V. Topping, J. M. Adam, F. J. Pallarés, R. Bru, and M. L. Romero, eds., Saxe-Coburg Publications, Stirlingshire, UK, 75–112.

Chandrashekhara, K., Krishnamurthy, K., and Roy, S. (1990). "Free vibration of composite beams including rotary inertia and shear deformation." *Comput. Struct.*, 14(4), 269–279.

Craig, R. R., Jr. (1981). *Structural dynamics*, Wiley, New York.

Dancila, D. S., and Armanios, E. A. (1998). "The influence of coupling on the free vibration of anisotropic thin-walled closed-section beams." *Int. J. Solids and Struct.*, 35(23), 3105–3119.

Demasi, L. (2007). "Investigation of conditions of minimum induced drag of closed wing systems and C-Wings." *J. Aircr.*, 44(1), 81–99.

Eisenberger, M., Abramovich, H., and Shulepov, O. (1995). "Dynamic stiffness analysis of laminated beams using a first order shear deformation theory." *Compos. Struct.*, 31(4), 265–271.

El Fatmi, R., and Ghazouani, N. (2010). "Higher order composite beam theory built on Saint-Venants solution. I: Theoretical developments." *Compos. Struct.*, 10.1016/j.compstruct.2010.08.024.

Eslimy-Isfahany, S. H. R., and Banerjee, J. R. (2000). "Use of generalized mass in the interpretation of dynamic response of bending-torsion coupled beams." *J. Sound Vib.*, 238(2), 295–308.

Euler, L. (1744). *De curvis elasticis*, Bousquet, Lausanne and Geneva.

Frediani, A., Montanari, G., and Pappalardo, M. (1999). "Sul problema di prandtl della minima resistenza indotta di un sistema portante." *Proc. of XV AIDAA*, Associazione Italiana di Aeronautica e Astronautica, Rome, Italy, 267–278.

Ganesan, R., and Zabihollah, A. (2007). "Vibration analysis of tapered composite beams using a higher-order finite element. I: Formulation." *Compos. Struct.*, 77(3), 306–318.

Gundlach, J. IV, et al. (2000). "Multidisciplinary design optimization of a strut-braced wing transonic transport." *Proc. 38th Aerospace Sciences Meeting and Exhibit*, American Institute of Aeronautics and Astronautics, Reston, VA.

Kameswara Rao, M , Desai, Y. M., and Chitnis, M. R. (2001). "Free vibrations of laminated beams using mixed theory." *Compos. Struct.*, 52(2), 149–160.

Kant, T., Marur, S. R., and Rao, G. S. (1997). "Analytical solution to the dynamic analysis of laminated beams using higher order refined theory." *Compos. Struct.*, 40(1), 1–9.

Kapania, K., and Raciti, S. (1989). "Recent advances in analysis of laminated beams and plates. I: Shear effects and buckling." *AIAA J.*, 27(7), 923–935.

Kiani, K., Nikkhoo, A., and Mehri, B. (2009). "Prediction capabilities of classical and shear deformable beam models excited by a moving mass." *J. Sound Vib.*, 320(3), 632–648.

Marur, S. R., and Kant, T. (1996). "Free vibration analysis of fiber reinforced composite beams using higher order theories and finite element modelling." *J. Sound Vib.*, 194(3), 337–351.

McCarthy, T. R., and Chattopadhyay, A. (1998). "Investigation of composite box beam dynamics using a higher-order theory." *Compos. Struct.*, 41(3–4), 273–284.

McConnell, K. G. (1995). *Vibration testing: theory and practice*, Wiley, New York.

Novozhilov, V. V. (1961). *Theory of elasticity*, Pergamon Press, Oxford.

Reddy, J. N. (2004). *Mechanics of laminated composite plates and shells: Theory and analysis*, 2nd Ed., CRC Press, Boca Raton.

Senjanović, I., and Fan, Y. (1989). "A higher-order flexural beam theory." *Comput. Struct.*, 32(5), 973–986.

Shi, G., and Lam, K. Y. (1999). "Finite element vibration analysis of composite beams based on higher-order beam theory." *J. Sound Vib.*, 219(4), 707–721.

Song, O., and Librescu, L. (1993). "Free vibration of anisotropic composite thin-walled beams of closed cross-section contour." *J. Sound Vib.*, 167(1), 129–147.

Song, S. J., and Waas, A. M. (1997). "Effects of shear deformation on buckling and free vibration of laminated composite beams." *Compos. Struct.*, 37(1), 33–43.

Simsek, M., and Kocatürk, T. (2007). "Free vibration analysis of beams by using a third-order shear deformation theory." *Sadhana-Acad. Proc. Eng. Sci.*, 32(3), 167–179.
Timoshenko, S. P. (1921). "On the corrections for shear of the differential equation for transverse vibrations of prismatic bars." *Philosophical Magazine*, 41, 744–746.
Timoshenko, S. P. (1922). "On the transverse vibrations of bars of uniform cross section." *Philosophical Magazine*, 43, 125–131.
Timoshenko, S. P., and Goodier, J. N. (1970). *Theory of elasticity*, McGraw-Hill, New York.
Tsai, S. W. (1988). *Composites Design*, 4th Ed., Think Composites, Dayton.
Wolkowich, J. (1986). "The joined-wing: An overview." *J. Aircr.*, 23(3), 161–178.
Yu, W., and Hodges, D. H. (2005). "Generalized Timoshenko theory of the variational asymptotic beam sectional analysis." *J. Am. Helicopter Soc.*, 50(1), 46–55.